Deep Space Navigation Augmentation Using Variable Celestial X-ray Sources

Suneel I. Sheikh, *ASTER Labs, Inc.*
John E. Hanson, *CrossTrac Engineering*
John Collins and Paul Graven, *Microcosm, Inc.*

BIOGRAPHY

Suneel Sheikh is CEO & Chief Research Scientist at ASTER Labs, Inc. He received his Ph.D. in 2005 from the University of Maryland, where his dissertation investigated the use of X-ray pulsars for spacecraft navigation. Prior to this, he has over ten years of industry experience in inertial navigation systems and GPS integration research.

John Hanson is the President of CrossTrac Engineering, Inc. In 1996 he received his Ph.D. in Aerospace Engineering from Stanford University. As a member of the Argos/USA team, his dissertation focused on the use of X-ray pulsars for spacecraft attitude, position, and time determination. He has been working in the spacecraft navigation and system design field for the past fifteen years.

John Collins is a Senior System Engineer with Microcosm, Inc. He manages technology development efforts for spacecraft GN&C components, and performs mission and system engineering tasks. He received his BS degrees in Aeronautical/Astronautical Engineering and Astronomy from the University of Illinois.

Paul Graven is the Director of Technology Development at Microcosm, in Hawthorne CA. Prior to joining Microcosm he spent five years as a management consultant developing growth strategies for early stage technology companies and 10 years as a GN&C engineer with TRW. He received his MS in Aeronautics & Astronautics from Stanford University, his BS in Engineering & Applied Science, and Economics from Caltech and a Master's in Public Policy from Harvard University's John F. Kennedy School of Government.

ABSTRACT

The accurate determination of navigation solutions for deep space exploration spacecraft is a crucial element of mission operation. These solutions are necessary to ensure successful arrival at the intended destination, to maintain continuous communication between Earth tracking stations and the remote vehicle, and for certain missions to monitor the position of the vehicle during its lifetime. The NASA Deep Space Network (DSN) has provided this capability for numerous missions beyond the Earth-Moon system. As more missions are planned and DSN availability becomes constrained, additional methods to maintain accurate navigation solutions, which would reduce the reliance on continuous vehicle tracking and monitoring, become attractive. The development of space vehicle navigation using variable celestial X-ray sources could potentially provide this additional capability, by providing supplementary external measurements that can be processed as part of the orbit determination algorithm in the mission control centers. This new technique also has the potential of providing autonomous navigation abilities via computation onboard the vehicle. These solutions can be used directly for guidance and control.

Overviews of the DSN system and the X-ray navigation technology are provided. The development of an integrated navigation system, including an extended Kalman filter that incorporates the spacecraft dynamics and measurements from both types of systems is presented. A simulation is presented that has been produced to investigate the potential of DSN location measurements that are augmented with X-ray source range measurements. Performance capabilities of each separate system and a combined system are provided.

INTRODUCTION

Past deep-space navigation techniques have primarily been provided by the NASA Deep Space Network (DSN), which produces precise spacecraft range and range-rate that are utilized to compute accurate three-dimensional position and velocity solutions. DSN relies on tracking stations affixed on Earth, thus the service generates less-accurate measurements perpendicular to the line of sight to a vehicle. Techniques such as delta differential one-way range (ΔDOR) have been demonstrated to mitigate a

large portion of these off-axis errors. It has been shown that the DSN using newer techniques can provide accurate position and velocity solutions, with approximately 2 nrad angular measurements – about 0.3 km of position error per astronomical unit (1 AU = 149,598,00 km) of distance from Earth. However, due to the expected demands on this service for future missions, developing methods to assist the DSN techniques by augmenting its solution with additional measurements can help improve DSN operations, primarily by reducing the frequency and duration of DSN observation required to maintain accurate solutions. Thus for further improvement, new techniques that would augment the DSN signals for use by vehicle's on interplanetary missions are of continued interest. For viability to future operational implementation, performance would be expected to maintain or improve upon current DSN capabilities.

Emerging technology and analysis has identified the use of variable, celestial X-ray sources, including rapidly spinning neutron stars, or *pulsars*, as potential navigation aids for spacecraft. These unique stars emit radiation throughout the electromagnetic spectrum, however the use of X-radiation is advantageous for spacecraft operations since smaller detectors can be utilized when compared to optical or radio-band instruments. Although theorized to exist for nearly a century, pulsars have only been detected and catalogued for the last 40 years. A subset of catalogued sources has been shown to produce variable signals with remarkable stability, with several objects achieving the stability of today's atomic clocks. Pulse timing models have been created using the stable, periodic signals from these sources. Along with these predictable pulse models, the spatial diversity of X-ray sources throughout the sky allows full three-dimensional position and velocity solutions to be generated for spacecraft on deep-space interplanetary trajectories.

Previous research has shown that the achievable navigation performance using these sources can be on the order of existing navigation technologies. Top-level error budgets and detailed dynamics simulations show that near autonomous onboard navigation solutions could be created using these sources alone. Much of this previous work, however, has concentrated upon improvements to solutions of vehicles in orbit about planetary bodies, specifically about Earth. In these cases, the cyclic nature of orbits about planets with well-defined gravitational fields considerably aids the maintenance of accurate position and velocity solutions. Thus, observations from any external source, including those from pulsars, serve primarily to correct any unmodeled disturbances. In contrast, with deep-space trajectories where the orbit rarely repeats its path, such as hyperbolic escape trajectories, infrequent, external observations and unmodeled disturbances allow significant navigation errors to accumulate between measurements.

This paper presents new techniques to augment the DSN with signals from variable, celestial X-ray sources. This new study investigates previously identified navigation methodologies using these celestial X-ray sources applied to deep space interplanetary missions, with spacecraft effectively on large elliptical or hyperbolic, heliocentric orbits. This study includes several methods of using pulsar signals, including; *i*) an absolute range measurement, which compares a pulse time of arrival to the expected arrival time from an accurate pulse timing model, and *ii*) an incremental range, which tracks phase and frequency of the received signal and the measured deviation from expected values are interpreted as spacecraft motion. These additional measurements, which can be made off-axis to the Earth-to-spacecraft range vector, are integrated within a Kalman filter that includes the known orbit dynamics of the vehicle.

To demonstrate potential performance, a software program has been created that generates simulated deep-space trajectories. The gravitational effects of the Sun as the central body, all the major planets, and the Moon are incorporated into the vehicle dynamics, as well as solar radiation pressure force. Range, range-rate, and angular position measurements offered by DSN are simulated to provide a baseline estimate of expected navigation performance. New solutions are then generated using X-ray source measurements that augment the DSN computations. Variable observation lengths of X-ray source measurements are provided to demonstrate the capability of reduced DSN contact, and to compare to DSN-only solutions. X-ray source-only solutions are also simulated and compared against DSN-based solutions to evaluate the potential for a fully autonomous onboard navigation system.

It is anticipated that by adding X-ray source measurements to future missions, the DSN workload can be reduced without sacrificing navigation accuracy. Adding this additional capability to future planned missions would enhance vehicle autonomy. Developing this new X-ray source navigation technology will eventually enable missions to very deep space to regimes where DSN alone may be unable to provide an acceptable level of accuracy.

DEEP SPACE NETWORK OVERVIEW

The DSN is a system of tracking stations and data processing centers used to provide telecommunication and orbit determination of spacecraft on voyages far from Earth [1]. The concept and system began in 1957 originally to support initial Earth satellite monitoring for the U.S. Army, and has grown through the past five decades to become the world's primary deep space communications and navigation system, supporting U.S.

and international expeditions to all solar system planetary bodies and beyond [2]. The DSN is primarily controlled and operated by the NASA Jet Propulsion Laboratory (JPL) in Pasadena, CA.

The primary purpose of the DSN is to provide two-way communication and data transfer between mission control centers located on Earth and the mission's spacecraft, planetary rover, or aero-vehicle. This communication process provides remote vehicle control and guidance, as well as vehicle health monitoring and status information. Data recorded by the mission instruments are transmitted from the vehicle to the data control center, and eventually to the mission project scientists. The spacecraft tracking process also provides vehicle orbit determination capabilities, which include monitoring and computing any required corrections to onboard oscillators, or clocks, used to define mission time and coordinate mission events. Using the measured signals between the tracking stations and the spacecraft, three-dimensional position and velocity orbit determination is performed, or surface location determination in the case of a planetary rover. The post-processed navigation solutions can then be utilized by mission coordinators to assess the vehicle's location along a planned trajectory and assist with performing any trajectory correction maneuvers (TCMs) as required.

Example popular missions directly supported by the DSN have been the Pioneer series of spacecraft to study the Moon, Jupiter, Saturn, and Venus; the Voyager 1 and 2 spacecraft to study Jupiter, Saturn, and the outer solar system; Galileo spacecraft designed primarily to study the Jupiter planetary system; Cassini spacecraft designed primarily to study the Saturn system; and recently the Mars exploration missions, including the Spirit and Opportunity surface rovers. As the Pioneer and Voyager spacecraft continue their journeys outward of the solar system towards the heliopause, the boundary where the Sun's solar wind is stopped by the interstellar medium, the DSN has maintained tracking of these vehicles during their extensive missions. Historically, DSN has been focused on supporting missions from Earth that extend beyond the Moon's orbit.

The DSN is comprised of three primary segments, including; the separate tracking stations with their signal processing centers; the data relay segments between stations and the control center; and the primary Network Operations and Control Center at JPL. The three tracking stations are located roughly 120° apart in longitude about Earth, which can provide near continuous tracking and observation coverage of any inertial location in space while subject to Earth's rotation. These stations are the Goldstone Deep Space Communications Complex (DSCC), Barstow, CA; the Madrid DSCC, just west of Madrid, Spain; and the Canberra DSCC, just southwest of Canberra, Australia. These three complexes are shown in Figure 1, with the chosen locations providing some natural terrain shielding of radio frequency interference. The tracking antennas at each location operate in the radio frequency band of the electromagnetic spectrum, and each complex has several antennas of various dimensions, including 26, 34, 64, and 70 m diameter antenna apertures. From a spacecraft's limited transmission power – typically 20 W – their signal must be concentrated into narrow beam widths. Even with a high gain antenna on the spacecraft, the received signal power at Earth is on the order of 10^{-20} W or lower. Using these large aperture antenna dishes assists with this low signal detection [2]. The three radio bands utilized by the system are the S-band (uplink = 2110-2120 MHz, downlink = 2290-2300 MHz), X-band (uplink = 7145-7190 MHz, downlink = 8400-8450 MHz), and the Ka band (uplink = 34.2-34.7 GHz, downlink = 31.8-32.3 GHz) [3]. The DSN system has evolved from the lower frequency S-band to higher Ka-band primarily to provide improved communications performance. In addition, the higher frequencies increase radiometric measurement accuracy by their shorter wavelengths, and are less susceptible to charged particle effects in Earth's upper atmosphere and the interplanetary solar plasma [3].

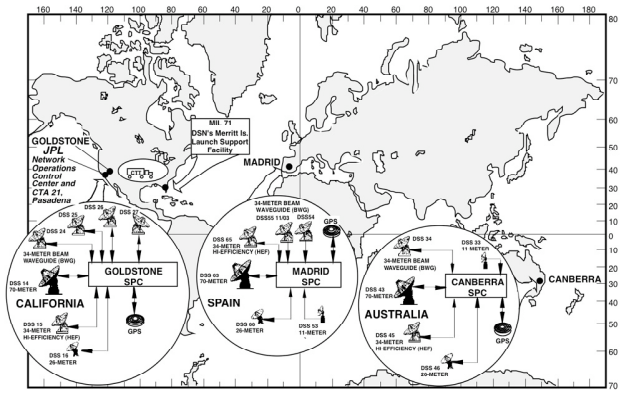

Figure 1. DSN three tracking station complexes (NASA diagram [1]).

Accurate tracking, communication, and orbit determination of the space vehicle requires high-quality reference data. These include accurate reference time, and the use of coordinate time scales such as UTC, TDG & TCG, and TDB & TCB [4]; accurate Earth and celestial reference frames, such as Earth-Centered Inertial (ECI), and International Celestial Reference Frame (ICRF), and accurate planetary ephemerides, which would include all major solar system bodies [5]. The DSN has also used the Global Positioning System (GPS) at all of its complexes and control centers to provide accurate, continuous high precision antenna location information and external time reference [6]. Ensembles of accurate, stable oscillators and frequency references are required at each tracking complex to maintain precise tracking of spacecraft signals.

The DSN has designed and utilized multiple techniques to track spacecraft signals and compute the observable range, range-rate, and angular position data [3, 7]. The *one-way tracking* method is achieved by a spacecraft producing a downlink signal to the tracking station. This signal is generated using an oscillator onboard the vehicle. No radio transmission is sent up to the vehicle in this approach. The *two-way tracking method* is achieved by transmitting an uplink signal to a spacecraft and then receiving the spacecraft's downlink signal at the same tracking antenna. Since the same tracking station frequency reference is used for the uplink and downlink signal tracking, this approach can be very accurate. However this approach can only be achieved when the round trip light time (RTLT) is less than the available spacecraft visibility time at the station as Earth rotates. Assuming the visibility time is eight hours at each of the three stations on Earth, this approach is not possible at distances greater than 29 AU, or beyond the orbit of Neptune. Thus, in the *three-way tracking* approach, the uplink signal is transmitted to a spacecraft from one tracking station and the downlink signal is received from the spacecraft at another tracking station site.

A range measurement is performed by tracking a ranging signal, which is transmitted by the spacecraft in the one-way tracking method or by the tracking station in the two- or three-way tracking methods. This ranging signal is a series of sinusoidal tones produced by the transmitters frequency reference and is phase modulated onto the transmitting carrier signal [3]. The receiver locks onto the signal via a phase-locked loop, and the received range code is compared against the transmitted range code in order to compute the RTLT. These range measurements are quantized in units known as range units and are dependent on the frequency of the highest component of the code. The range units are currently quantized at 28 cm [3]. Similarly, the Doppler shift measurement can be produced by comparing the frequency of the received reference signal with the station's frequency reference. Newer DSN implementations use pseudo-random noise – similar to GPS – instead of a sequence of sinusoidal tones. This allows for greater distance range measurements at lower power.

Accurate orbit determination of spacecraft using the DSN is performed by measuring the slant range and range-rate, and the angular position if possible, between a tracking station's antenna and the interplanetary spacecraft. Using multiple range and range-rate measurements, in addition to the modeled vehicle dynamics that includes all necessary acceleration perturbations, the orbit parameters can recursively be updated in order to maintain accurate post-processed solutions of vehicle inertial position and velocity. The range observable is computed as,

$$\rho = c\Delta t \tag{1}$$

where, ρ is the slant range between the tracking antenna and the spacecraft, c is the speed of light, and Δt is the elapsed time of the signal transit from the spacecraft to the antenna. This elapsed time is also referred to as the *one-way signal transit* time [3]. The range-rate observable is computed from,

$$\dot{\rho} = c\left(1 - \frac{f_R}{f_T}\right) \tag{2}$$

where, $\dot{\rho}$ is the range-rate term, f_R is the received frequency from the spacecraft at a tracking antenna on Earth, and f_T is the frequency transmitted by the spacecraft. As the spacecraft recedes away from Earth, its transmitted frequency, or tone, is shifted due to the Doppler effect, as

$$f_R = c\left(1 - \frac{\dot{\rho}}{c}\right) f_T \tag{3}$$

The $\dot{\rho} f_T / c$ is referred to as the Doppler shift term. Eqs. (1) through (3) are simplified forms of the true measurement relationships, which require precise geocentric station coordinates, Earth rotation effects, and Earth and celestial reference frame transformations in order to produce data within the proper inertial reference frame for the orbit determination process.

The addition of angular position measurements of the spacecraft in terms of right ascension, α, and declination, δ, determined by the tracking station on Earth can contribute significantly to the calculation of high performance orbit determination solutions. Range and range-rate measurements essentially only provide one- or two-axis of position and velocity information. Thus, many sequential range and range-rate measurements would be required to resolve the remaining axes for full three-dimensional solutions. Very long baseline interferometry (VLBI) techniques adopted in the 1970's can provide the angular position data with high accuracy. In this approach, observations by tracking stations antennas with known, well-surveyed relative locations between each of them on Earth are used to simultaneously track the downlink signal from spacecraft, and the differential time delay measured between these stations provides a measure of the relative angle between stations and the arriving planar wave from the spacecraft [8], as shown in Figure 2. If both stations are tracking the same spacecraft and the baseline between stations is perpendicular to the spacecraft's transmitted signal, then there will be no signal delay detected between stations. If the baseline is at some angle with respect to the incoming signal, then some delay between these tracking antennas will be detected that can be used as a measure of this spacecraft offset angle, θ_{SC}, as,

$$\Delta\rho_{AB} = \rho_A - \rho_B = c\left(\Delta t_A - \Delta t_B\right) = \mathbf{b}\cdot\hat{r} = \left\|\mathbf{b}\right\|\sin\theta_{SC} \tag{4}$$

where, $\Delta\rho$ is the range difference between stations A and B, Δt_A and Δt_B are the signal transit time from the spacecraft to stations A and B respectively, $\mathbf{b}$ is the

baseline vector between stations A and B, and $\hat{r}$ is the unit vector towards the spacecraft. After any signal integer cycle ambiguities have been resolved within the range delay of the VLBI measurements, this differenced, or differential, one-way range (DOR) measurement is used to compute the angular position of the spacecraft.

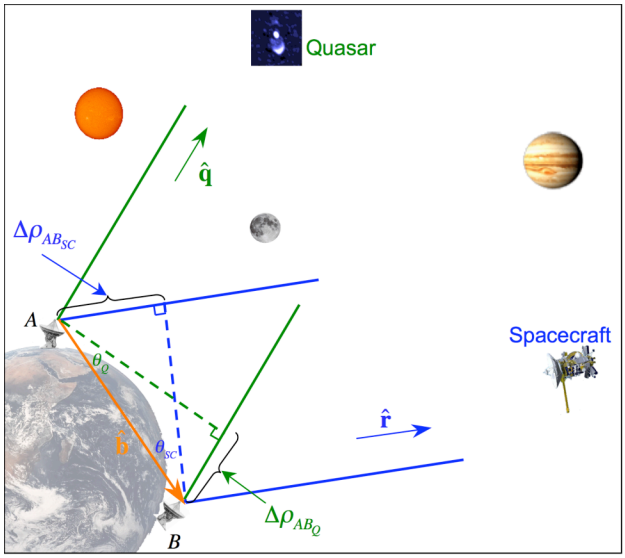

Figure 2. DSN observations of remote spacecraft and radio source.

To further improve the spacecraft's angular position measurements, by simultaneously observing a secondary radio source that is at a known sky position, the systematic errors in the DSN VLBI measurements that are common for the radio source and spacecraft observations can be effectively removed. This approach has been demonstrated to be very effective using cataloged celestial radio sources, including quasars. The angular position knowledge of many of these catalogued sources determined in the ICRF frame is 5 nrad or better [3]. By differencing both of the DOR measurements from the radio source and spacecraft observations, this delta-DOR, or ΔDOR, computation can provide an improved angular position measurement of the spacecraft using,

$$\Delta\rho_{AB_{SC}} - \Delta\rho_{AB_Q} = \mathbf{b}\cdot\hat{r} - \mathbf{b}\cdot\hat{q} = \|\mathbf{b}\|\left(\sin\theta_{SC} - \sin\theta_Q\right) \quad (5)$$

In this expression, although no error terms are listed, the terms for the quasar, $\Delta\rho_{AB_Q}$, $\hat{q}$, and θ_Q, are known to high precision, thus the offset angle of θ_{SC} can be determined with high accuracy. Common system errors such as each tracking station's clock offsets and instrumentation delays can be effectively removed, while errors such as uncalibrated atmospheric effects and baseline errors can be reduced [3].

Performance of the DSN spacecraft position and velocity determination has improved as the system has evolved over the past decades. Early range and range-rate accuracies were many meters and fractions of a cm/s, but have now approached 1-m and 1-mm/s. Angular position uncertainties were originally 100-nrad, but have been reduced to approximately 2-nrad today [9, 10]. The frequency of DSN measurements varies from as little as once per week for interplanetary cruise phase of a trajectory, to one to three times per day prior to TCM or planetary rendezvous.

Although the achieved performance values are remarkable, limitations of the DSN exist that constrain the observable range, range-rate, and angular position accuracies [3]. System errors such as clock instabilities both on the remote spacecraft and at the tracking stations reduce the ability to produce accurate frequency references; station instrument errors such as electronics group delays introduce range error; and transmission media, including the interplanetary medium and Earth's troposphere and ionosphere cause dispersive signal delays. Tracking station platform errors, such as the precise antenna phase center on Earth's movable crust plates; Earth's reference frame; and precession and nutation of Earth's polar axis, all contribute to receiving station location errors. Precise time standards also have errors that accumulate over time, such at UTC. Uncertainties in the planetary ephemerides, including angular position knowledge of solar system bodies, create unmodeled perturbation effects on spacecraft orbit dynamics. Celestial radio source catalogued position errors affect VLBI and ΔDOR measurement accuracies.

In addition to the DSN system and parameter errors, external pressures on the operational system can also affect potential performance. Tracking station availability and scheduling can become an issue with many supported missions. With newly planned exploration missions, it is expected by 2020 that DSN will be required to support nearly twice as many missions as supported in 2005. Maintenance and upkeep of the various stations and antennas can consume operating funds. Ongoing legacy missions require older systems and methods to remain intact; while newer missions require new methods and equipment to support increased data rate transfers and more precise orbit determination. The orbit determination procedure is a post-processed solution. Thus, real-time navigation is not provided for any proposed missions that may benefit from instantaneous position knowledge. Although the DSN continues to demonstrate its capability even while the Voyager spacecraft travel beyond the heliosheath nearing the outer boundaries of our solar system, the position uncertainty computed by the system increases as the spacecraft travels further from Earth.

X-RAY NAVIGATION OVERVIEW

The X-ray navigation (XNAV) concept provides a means for spacecraft to determine navigation solutions using variable celestial X-ray sources. Several early approaches

of position determination navigation using these sources were initially developed soon after the successful detection of these stars [11, 12]. More recent research has shown new methods to perform vehicle navigation based upon additional discoveries and detailed cataloguing of sources, as well as the continued development of more sensitive and finer time resolution detectors [13-16]. This research has shown that methods of time, attitude, position, and velocity determination are possible with this new, unique technology, and may eventually provide a fully autonomous planetary orbiting and interplanetary navigation technique.

The XNAV system is comprised of three primary components, including the set of visible celestial X-ray sources, an X-ray detector affixed onboard a spacecraft, and the externally observed parameter database of each source's characteristics. The X-ray sky contains several types of variable celestial objects that can be used for various aspects of spacecraft navigation, including neutron stars. Variable X-ray objects employ an array of energy sources for their X-ray emissions, and their variability is produced by *intrinsic* and *extrinsic* mechanisms. While all variable emission sources are good candidates for time, position, and/or velocity determination, those objects that produce nearly persistent, non-pulsating X-ray flux may be more beneficial candidates for attitude determination. Although variable celestial sources exist that emit in all bands of the electromagnetic spectrum, the primary advantage for spacecraft using X-ray type sources is that smaller sized detectors can be utilized. This offers significant savings in power and mass for spacecraft development and operations. Catalogued X-ray sources that have potential for navigation are plotted in Figure 3 [14, 15, 17].

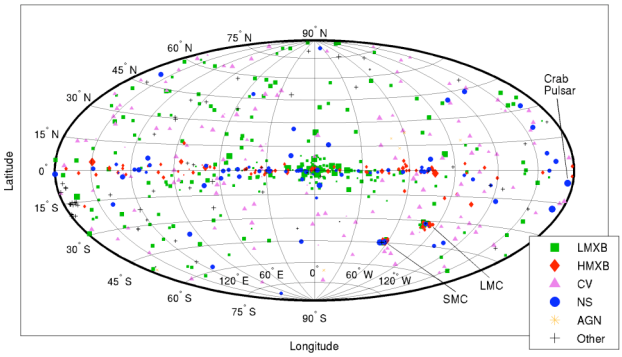

Figure 3. Plot of catalogued X-ray sources in Galactic longitude and latitude [15].

A neutron star (NS) is the result of a massive star that has exhausted its nuclear fuel and undergone a core-collapse resulting in a *supernova* explosion [18-20]. During their collapse, conservation of angular momentum spins these stars up to very high rotation rates. Young, newly born neutron stars typically rotate with periods on the order of tens of milliseconds, while older neutron stars through energy dissipation eventually slow down to periods on the order of several seconds. A unique aspect of this rotation is that it can be extremely stable and predictable. Neutron stars harbor immense magnetic fields. Under the influence of these strong fields, charged particles are accelerated along the field lines to very high energies, and powerful beams of electromagnetic waves are radiated out from the magnetic poles. X-rays, as well as other forms of radiation, can be produced within this magnetospheric emission. If the neutron star's spin axis is not aligned with its magnetic field axis, then an observer will sense a *pulse* of electromagnetic radiation as the magnetic pole sweeps across the observer's line of sight to the star, hence these sources are referred to as *pulsars*. Since their discovery in 1967 [21], pulsars have been found to emit throughout the radio, infrared, visible (optical), ultraviolet, X-ray, and gamma-ray energies of the electromagnetic spectrum. With their periodic radiation and wide distribution, pulsars appear to act as natural beacons, or *celestial lighthouses*, on an intergalactic scale. Due to their specific evolution, variability mechanisms, and geometric orientation relative to Earth, each pulse frequency and shape is a unique identifying signature for each star.

Many X-ray pulsars are *rotation-powered* pulsars. The energy source of these neutron stars is the stored rotational kinetic energy of the star itself. The X-ray pulsations occur due to two types of mechanisms, either *magnetospheric* or *thermal* emissions [22]. Some stars can emit using both types of mechanisms. *Accretion-powered pulsars* (APSR) are neutron stars in binary systems, where material is being transferred from the companion star onto the neutron star. This flow of material is channeled by the magnetic field of the neutron star onto the poles of the star, which creates hot spots on the star's surface. The pulsations are a result of the changing viewing angle of these hot spots as the neutron star rotates. Two types of APSRs are frequently catalogued based upon the mass of the orbiting companion of the neutron star, either a high-mass X-ray binary system (HMXB), where the companion object is typically 10–30 solar masses in size, or a low-mass X-ray binary system (LMXB), where the companion star is perhaps size of less than one solar mass [22, 23]. These types of pulsars also show signal stability and predictability. Although they possess complicated pulse timing models due to their binary system dynamics, and many are transient sources with unpredictable durations of low signal intensity, these types of pulsars also have characteristics conducive to navigation.

Pulsars are extremely distant from the solar system, which provides for good visibility of their signal near Earth as well as throughout the solar system. However unlike Earth satellite ranging systems, the distances of these sources cannot be measured such that direct range measurements from the sources to a spacecraft can be determined. Rather, indirect range measurements along the line of sight to a pulsar from a referenced inertial

location to a spacecraft are computed. The periodic pulsations from these sources essentially emulate celestial clocks. As select sources have had extended observations over many years, long-term data analysis has verified that the spin rates are extremely stable for some of these sources. Their stability has been shown to compare well to the stability of current day atomic clocks [24, 25]. This high stability allows for the accurate prediction of pulse arrivals and the creation of precise pulse timing models.

At X-ray energy wavelengths, the primary measurable values of the emitted signal from a source are the individual high-energy photons emitted by the source. The rate of arrival of these photons can be measured in terms of *flux* of radiation, or number of photons per unit area per unit time. The diffuse X-ray background is an appreciably strong signal that is observed when viewing the X-ray sky, and measures of this background radiation must be considered when observing a source [22]. However, the sources being observed are periodic so that frequency dependent techniques such as epoch folding and phase-locked loops can be used to extract seemingly small source signals from the noise that is created by the diffuse X-ray background and the shot noise associated with the pulsar signal itself.

This navigation concept is primarily driven by the unique, periodic, nature of the signal produced by these variable sources. By measuring the pulse time-of-arrival (TOA) from each source, this data can be related to a range measurement in order to be used to update or compute three-dimensional position and velocity solutions. As most current X-ray telescope and detector designs can observe only a single source along one point on the celestial sphere, navigation concepts that utilize single axis ranging information have shown that accurate orbit solutions can be achieved [15, 16]. Extensions to this single measurement have also been pursued, including approaches similar to Global Navigation Satellite Systems (GNSS), where multiple variable sources are used to compute full 3-D position solutions [26, 27]. These methods use lateration concepts to estimate the range from an inertial origin along multiple axes. As eventual detector systems may be produced that will monitor the whole sky, simultaneous observations of multiple source signals from different directions allow this concept to produce full 3-D solutions. Spacecraft that have accurate clocks onboard, can track these signals over time to maintain full dynamic trajectory solutions. It may be possible to further expand this concept and use the stable, periodic signals from these sources to produce accurate time as well as vehicle position, allowing complete navigation solutions without the need for an ultra-stable on-board clock.

The *profile* of each pulse from an X-ray source is a representation of the characteristics of the pulse. Pulse profiles vary in terms of shape, size, cycle length, and intensities. Some sources produce sharp, impulsive, high intensity profiles, while others produce sinusoidal, elongated profiles. Although many sources produce a single, identifiable pulse, other pulse profiles contain sub-pulses, that are evident within the signal [28, 29].

To observe a source, an X-ray detector is initially aligned along the line of sight to the chosen source. Various types of detectors have been used in X-ray astronomy missions depending on the type of application of timing or imaging, such as gas proportional counters with collimators or focusing optics with small solid state detectors [30]. Once photon events from this source are positively identified, components within the detector system record the time of arrival of each individual X-ray photon with respect to the system's clock to high precision. During the total observation time of a specific source, a large number of photons will have each of their arrival times recorded. The measured individual photon arrival times must then be converted from the detector's system clock to their coordinate time in an inertial frame. This conversion provides an alignment of the photon's arrival time into a frame that is not moving with respect to the observed source. This process of assembling all the measured photon events into a pulse profile is referred to as *epoch folding*, or averaging synchronously all the photon events with the expected pulse period of the source. For X-ray observations that record individual photon events, Poisson counting statistics typically dominate the random noise in pulse TOA computation. The time shift necessary to align the peaks within the observed profile and a standard pulse template is added to the start time of the observation to produce the absolute TOA of the pulse for a particular observation. An estimate of the accuracy of the TOA measurement can be computed as an outcome of this comparison process. This estimate provides an assessment on the quality of the TOA measurement, and can be useful in the navigation algorithms [31]. Figure 4 shows a standard pulse template for the Crab Pulsar (PSR B0531+21) in the X-ray band (1–15 keV) created using multiple observations with the USA experiment onboard the *ARGOS* vehicle [32]. This image shows two cycles of the pulsar's pulse for clarity. The Crab Pulsar's pulse is comprised of one main pulse and smaller secondary sub-pulse with lower intensity amplitude.

The pulsed emission from variable celestial sources arrives within the solar system with sufficient regularity that the arrival of each pulse can be modeled. These models predict when specific pulses from the sources will arrive within the solar system. Pulse timing models are often represented as the total accumulated phase of the source's signal as a function of time. A starting cycle number, $\Phi_0 = \Phi(t_0)$, can be arbitrarily assigned to the pulse that arrives at a fiducial time, t_0, and all subsequent pulses can be numbered incrementally from this first

pulse. Using the determined pulse frequency, f, and its derivatives, the total phase can be specified at a particular location using a pulsar phase model of,

$$\Phi(t) = \Phi(t_0) + f\left[t - t_0\right] + \frac{\dot{f}}{2}\left[t - t_0\right]^2 + \frac{\ddot{f}}{6}\left[t - t_0\right]^3 \quad (6)$$

Eq. (6) is known as the *pulsar spin equation*, or *pulsar spin down law* [28, 29]. In this equation, the observation time, t, is in *coordinate time*. The model shown in Eq. (6) utilizes frequency and two of its derivatives; however, any number of derivatives may be required to accurately model a particular pulsar's timing behavior. Additionally, sources that are components of multiple star systems, such as binary systems, require parameters that include the periodic orbits of the source within the systems. The data of the characteristics of several well-studied pulsars has been presented in past publications [15, 16, 33]. The accuracy of the pulse timing models depends significantly on whether the intrinsic nature of the source continues to match the model's predicted rotation rates. Precise external information is also required to complete an accurate timing measurement, such as Earth and celestial reference frames, planetary ephemerides, and coordinate time scales.

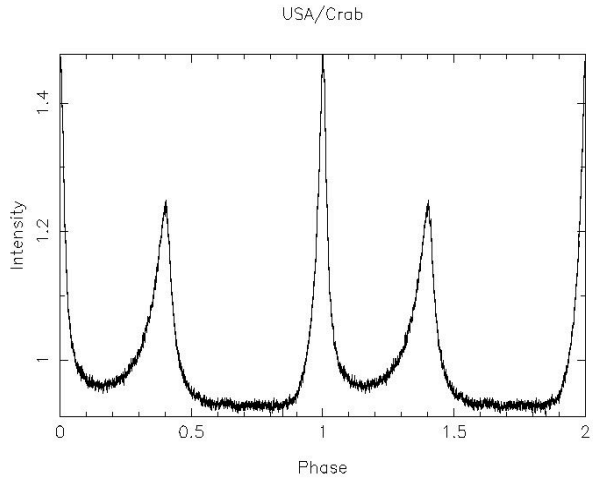

Figure 4. Crab pulsar standard pulse template. The period is about 33.5 milliseconds.

There are several methods of XNAV position and velocity determination that have been researched [14-16, 27]. They can be categorized in an *absolute* sense and a correction, or *delta-correction*, sense. In the absolute mode, methods are created to determine the absolute three-dimensional position and/or velocity in an inertial reference frame. In the delta-correction mode, updates to estimated position and velocity values are generated from the pulsar measurements. Either of these methods contributes to maintaining a continuous, accurate navigation solution.

Many of the previously published position determination corrections methods used the measured TOA from a pulsar to provide position, or range, information with respect to a specific origin, planetary body, or even another spacecraft. However, the goal of a full three-dimensional position determination process is to compute the three-axis location information with respect to an inertial origin without requiring knowledge of other nearby bodies or information in a relative sense. To compute this solution using pulsars, it is necessary to monitor several pulsars simultaneously and merge their pulse TOA information into a single solution [27]. This would require multiple X-ray detectors pointed towards all these individual sources, or a single X-ray detector system that has all-sky monitoring capabilities. Uncertainties in the pulse cycles with respect to the reference origin would exist and must be resolved to declare a solution valid [15, 27]. However, once the cycle ambiguities are resolved, continuous absolute position solutions would be possible. This concept is reminiscent of the similar concepts used to determine absolute navigation using the Earth-based GNSS, the absolute method of navigation using variable celestial sources is actually more challenging to implement, primarily due to the requirement of multiple detectors and processors.

A less complex concept to implement may be a single detector technique that provides corrections to estimated range solutions. The most common approach is the computation of a TOA-difference. When viewing a single pulsar, with its known pulse timing model, the computed TOA difference between the predicted TOA of the model and the measured TOA by the detector can be used to estimate the error in range along the line of sight to the source. Blending this range information with estimated position from an orbit propagator produces corrections to the position and velocity solution, which maintains accurate solutions over time. Figure 5 shows a conceptual illustration where arriving pulses are used to help update the spacecraft position with respect to the solar system barycenter reference frame. To produce accurate TOA measurements, long observation durations – many thousands of seconds – are required from sources based upon the error budget analysis or the Cramer-Rao lower bound achievable performance [33, 34].

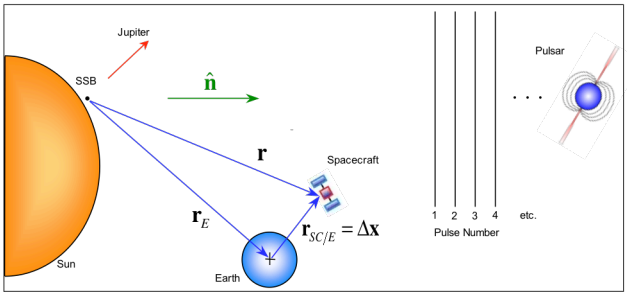

Figure 5. Position of spacecraft as pulses arrive into solar system from distant pulsar [15].

An alternative delta-correction technique that can potentially provide continuous update information versus the infrequent TOA-difference technique is the method of continuous phase tracking of a source while it is being observed [34, 35]. This method can estimate and lock onto the phase and frequency of a source based upon the known pulse-timing model. By tracking these expected

parameters of the source signal, an estimate of the spacecraft vehicle motion within its orbit in an inertial frame is produced. Thus, over short time intervals (tens of seconds), continuous updates of vehicle motion are estimated and many measurements are possible [34]. Digital phase-locked loops can be implemented to insure proper tracking of these signals.

Once measurements are produced from pulsar observations, effective techniques to incorporate this information must be designed within the spacecraft navigation system. The use of extended Kalman filters, which use the numerically integrated orbital dynamics of the spacecraft blended with pulsar observation measurements, has been proven very effective for this task [15, 16]. Errors within the position and velocity solutions have been correctly removed with these implementations, and filters such as these can be operated in real time onboard spacecraft for improved autonomous operations.

Several important limitations exist for the XNAV concept. A navigation system that utilizes pulsed emissions from pulsars would have to address the faintness, transient, flaring, bursting, and glitching aspects of these sources, in addition to the number of signal phase cycles received and the presence of the noise from the X-ray background, cosmic ray events, and detector noise [23]. An operational system would require a pulsar almanac database with current source characteristics and profile information. Due to the faintness of many of these sources, X-ray detectors with large effective collecting areas are required along with long observation durations, which comes as a tradeoff between available payload mass and power usage versus the overall mission spacecraft size and objective. A stable onboard clock would be an essential part of a complete XNAV system. Additionally, a full XNAV system has not been flight tested yet to date. Although data from actual X-ray astronomy missions have been used to demonstrate the capability, a dedicated flight experiment is yet to be built and flown.

AUGMENTED NAVIGATION APPROACH

Although the DSN provides navigation for almost all deep space missions, methods that provide augmentation to this service can help it offload potential oversubscription and increase operational vehicle autonomy. XNAV is a new technology that can potentially provide this augmentation and increased autonomy.

An integrated DSN and XNAV system would likely be initially operated as a post-processed orbit determination system, in a manner similar to the operational DSN as used today. A Kalman filter that accounts for the vehicle dynamics, known thrust maneuvers, and all modeled acceleration perturbations, including third-body planetary gravitational effects and solar radiation pressure, would be created that uses both time-tagged DSN range, range-rate, and angular position and XNAV range measurements. DSN measurements would be computed and processed as done today. To facilitate computing XNAV measurements, raw time-tagged photon events and source observation information from the onboard X-ray detector would be included as part of the downlink message from the spacecraft to the tracking station antenna. These photon events would be folded in the ground processing computers, and pulse TOAs computed to form range correction measurements. If photon events are too numerous to be efficiently sent in the communication signal, the pulse folding could be processed onboard the spacecraft, using its best-estimated navigation solution, to form simple pulse TOA values. If a digital PLL solution is implemented, the phase measurement from the PLL could be transmitted to the ground. In either case, on-board preprocessing of the source data would limit the impact of the XNAV system on the downlink data budget.

The goal of this augmented navigation solution would be to improve the navigation solution of either DSN or XNAV alone. For those spacecraft already using DSN tracking, the additional range, range-rate, and angular position measurements from this Earth-based service would combine well with XNAV solutions to improve the overall navigation accuracy [36, 37]. In addition, the three solutions of DSN-only, XNAV-only, and DSN+XNAV would provide a level of verification for each of these systems.

SIMULATION DESCRIPTION

To support the analysis of these augmented navigation systems, a simulation program has been developed that provides a working environment for test and verification. This simulation emulates the dynamics of interplanetary vehicle trajectories and uses these data to operate a fully combined DSN and XNAV EKF.

The design and development of this simulation follows the treatment previously presented in references [15, 16]. The dynamics of the position and velocity states of the vehicle are propagated along fixed time steps using the integration of vehicle velocity and acceleration. The system is represented by the state vector, $\mathbf{x}$, which has a total of six states, and is composed of the three element spacecraft (SC) position vector, $\mathbf{r} = \mathbf{r}_{SC} = \left\{ r_x, r_y, r_z \right\}^T$, and the three element spacecraft velocity vector, $\mathbf{v} = \mathbf{v}_{SC} = \left\{ v_x, v_y, v_z \right\}^T$. The dynamics of this non-linear orbit propagation system is represented as,

$$\dot{\mathbf{x}}(t) = \bar{f}\left(\mathbf{x}(t), t\right) + \boldsymbol{\eta}(t) = \begin{bmatrix} \dot{\mathbf{r}} \\ \dot{\mathbf{v}} \end{bmatrix} = \begin{bmatrix} \mathbf{v} \\ \mathbf{a} \end{bmatrix} \tag{7}$$

In this equation, $\vec{f}$ is the non-linear function of the state vector. The second term in Eq. (7), $\boldsymbol{\eta}(t)$, is the noise vector associated with the unmodeled state dynamics. The values of these states can be determined over all time t_0 to t with a known model of vehicle acceleration, **a**, and an initial condition value at epoch t_0 of $\mathbf{x}_0$. The acceleration is dynamically modeled similarly to the acceleration presented in these references; however, with the exceptions this analysis uses non-periodic heliocentric interplanetary orbits, with the Sun as the central gravitational field, includes solar radiation pressure as a perturbing force, and considers the third-body effects of all nine planets and the Moon. The total acceleration of the spacecraft in these orbits is the sum of these effects as,

$$\mathbf{a}_{total} = \ddot{\mathbf{r}} = \mathbf{a}_{Sun} + \mathbf{a}_{solar\,radiation} + \mathbf{a}_{third-body} + \mathbf{a}_{H.O.T} \quad (8)$$

The simulation includes solar radiation pressure force only when the spacecraft is in full sunlight view, and not when it is in the shadow of a planetary body. Any higher order terms (H.O.T.) that are not modeled but relevant for a specific missions (such as atmospheric drag) would be included as needed. To maintain high accuracy, an 8th order Runge-Kutta integration routine is utilized for the state vector integration, which requires ten function evaluations from Eq. (7) for each time step iteration [38]. The ICRF reference frame is used for these trajectories [4], and the DE405 planetary ephemeris provides location information of each body [5]. A *truth* navigation solution is propagated using these dynamics and begins with exact initial state vector conditions. A *simulated* solution is propagated using the same dynamics but with some initial condition error. Left uncorrected, this simulated navigation solution would diverge from the true solution over time.

Two extended Kalman filters (EKF), due to the non-linear state dynamics, have been developed to analyze the performance of the DSN and XNAV under the same operating and trajectory path conditions. The simulation can operate each of the filters independently, or as a combined system processing both types of measurements. Each filter uses errors of the position and velocity state vector as its filters states.

The error-states, $\delta\mathbf{x}$, can be represented based upon the true states, **x**, and the estimated states, $\tilde{\mathbf{x}}$, as,

$$\mathbf{x} = \tilde{\mathbf{x}} + \delta\mathbf{x} \quad (9)$$

Necessary for error-state and error-covariance processing within each EKF is the proper representation of the state transition matrix, $\boldsymbol{\Phi}$. This matrix is used to determine the values of the error-state at a future time, t.

$$\delta\mathbf{x} = \boldsymbol{\Phi}\left(t, t_0\right)\delta\mathbf{x}_0 \quad (10)$$

Each of the EKF implementations follows the same evaluations as presented in references [15, 16]. The filter state propagation and the state transition matrix use the state dynamics and the differentials of this dynamics with respect to the states from the Eq. (8). An 8th order Runge-Kutta integration routine is also used for the propagation of these error states. The process noise for the covariance matrix propagation is modeled using a single spectral amplitude term of $S_p = 10^{-13}$ km^2/s^3 for the position and velocity states [39]. Measurements for the DSN and XNAV systems are processed as would be received by a full processing filter. During a measurement update, those measurements that pass their measurement residual test that are two times less than the innovations of the filter are processed, otherwise they are rejected. Simulated measurements, $\mathbf{y}(t)$, are created using the truth solution data with representative noise, $\boldsymbol{\nu}(t)$ added to emulate actual measurement values. The estimated measurement, $\vec{h}(\tilde{\mathbf{x}})$ is a function of the propagated state vector. The observations in terms of the error-states within each EKF is a measurement difference, **z**, as

$$\begin{aligned}\mathbf{z}(t) &= \mathbf{y}(t) - \vec{h}(\tilde{\mathbf{x}}) = \frac{\partial \vec{h}(\tilde{\mathbf{x}})}{\partial \mathbf{x}}\delta\mathbf{x} + \boldsymbol{\nu}(t) \\ &= \mathbf{H}(\tilde{\mathbf{x}})\delta\mathbf{x} + \boldsymbol{\nu}(t)\end{aligned} \quad (11)$$

In this representation, the measurement matrix, **H**, is composed of the partial derivatives of the measurement with respect to the state vector elements.

Latency in observation time is ignored within the simulation. To be fully implemented, these filters would be processed within ground control centers, with time-tagged data from both DSN and XNAV. The implementation of the simulation presented here has simplified this issue by assuming the measurements are produced at the time they are received. However, time alignment of data is an important issue not so easily ignored in a real-world implementation of this concept.

The DSN EKF simulation allows the user to select several parameters such as the type of measurement, either *range-only*; *range and range-rate,* or *range*; *range-rate, and angular position (ΔDOR)*, how often measurements are computed, e.g. *three per day*; *once per day*; or *once per week*, the time step and duration of the simulated trajectory, and an initial state vector, $\mathbf{x}_0$, that defines the orbit.

The DSN measurements are processed through the EKF using the observation measurement $\mathbf{y}(t)$, with added associated noise, and the estimated measurement using state values, $\vec{h}(\tilde{\mathbf{x}})$. For a ΔDOR measurement, the range and angular position observations can be interpreted as a three dimensional position measurement directly from Earth to the spacecraft. In terms of the spacecraft's relative position with respect to Earth, $\mathbf{r}_{SC/E}$, this ΔDOR measurement can be expressed as the following,

$$\mathbf{y}(t) = \mathbf{r}_{SC/E} + \boldsymbol{\nu}_{position} \quad (12)$$

$$\mathbf{h}(t) = \tilde{\mathbf{r}}_{SC/E} \quad (13)$$

$$\mathbf{H} = \begin{bmatrix}\mathbf{I}_{3\times3} & \mathbf{0}_{3\times3}\end{bmatrix} \quad (14)$$

The observation measurement noise is simulated using 1-m range and 2-nrad angular position measurement accuracy. Since these errors are expressed along essentially the radial, along-track, and cross-track (RAC) directions from Earth, the measurement noise can be simulated as,

$$\boldsymbol{\nu}_{position} = \mathbf{T}_{RAC}^{RV} \begin{bmatrix} \varepsilon_{range} & r_{SC/E}\varepsilon_{angle} & r_{SC/E}\varepsilon_{angle} \end{bmatrix} \quad (15)$$

where $\mathbf{T}_{RAC}^{RV}$ is the transformation matrix between the RAC and inertial position and velocity (RV) frame [40], and $\varepsilon_{\text{range}}$ and $\varepsilon_{\text{angle}}$ errors are based upon the one-sigma uncertainties along the radial and angular position directions, respectively. All noise errors in the simulation are created using the one-sigma uncertainty in the term multiplied by a normalized random number with zero mean and a standard deviation of one.

A range-rate measurement is expressed by incorporating the spacecraft's relative velocity with respect to Earth, $\mathbf{v}_{SC/E}$, along the radial unit direction, $\hat{\mathbf{r}}_{SC/E}$, as,

$$y(t) = \hat{\mathbf{r}}_{SC/E}^{T}\mathbf{v}_{SC/E} + \nu_{rate} \quad (16)$$

$$h(t) = \tilde{\hat{\mathbf{r}}}_{SC/E}^{T}\tilde{\mathbf{v}}_{SC/E} \quad (17)$$

$$\mathbf{H} = \begin{bmatrix} \dfrac{\left(\tilde{\mathbf{r}}_{SC/E}^{T}\tilde{\mathbf{r}}_{SC/E}\right)\tilde{\mathbf{v}}_{SC/E} - \left(\tilde{\mathbf{r}}_{SC/E}^{T}\tilde{\mathbf{v}}_{SC/E}\right)\tilde{\mathbf{r}}_{SC/E}}{\left\|\tilde{\mathbf{r}}_{SC/E}\right\|^{3}} & 0_{1\times 3} \end{bmatrix} \quad (18)$$

The magnitude of the range-rate measurement noise is simulated using 1-mm/s. Since the EKF states are heliocentric position and velocity, Earth position and velocity must be removed from the state terms to compute the geocentric values used in Eqs. (12) – (18).

The XNAV EKF simulation allows the user to select the same orbit and simulation parameters as the DSN EKF. However, the XNAV algorithm can be operated on either *absolute range* or *delta-phase range* measurements, as selected by the user. The implementation of the XNAV measurements is processed assuming the individually measured photon arrivals have been processed into a range-like measurement. The pulsar visibility is also verified to ensure that any solar system body from the spacecraft's location does not obscure the source. If the source is obscured, no measurement will be available until the spacecraft exits the body's shadow with respect to the source.

The absolute range observations measurements are processed as presented in references [15, 16], and includes the relativistic effects as shown there.

The delta-phase range observation measurements are expressed as the following,

$$y(t) = \hat{\mathbf{n}}_i^{T}\left[\mathbf{r}_{SC/S}(t_{k-1})\right] + \Delta\phi\left(t_{k-1} \rightarrow t_k\right) + \nu_{delta-phase} \quad (19)$$

$$h(t) = \hat{\mathbf{n}}_i^{T}\tilde{\mathbf{r}}_{SC/S} \quad (20)$$

$$\mathbf{H} = \begin{bmatrix} \hat{\mathbf{n}}_i & \mathbf{0}_{1\times 3} \end{bmatrix} \quad (21)$$

This observation is evaluated as the absolute position plus the delta-range change along the line of sight to the i^{th} pulsar, $\hat{\mathbf{n}}_i$, from time $t_{k\text{-}1}$ to t_k, represented as delta-phase, $\Delta\phi$. This observation could also be expressed as the incremental change in position along this line of sight by instead using only the phase term for $y(t)$ and the position change of $\left[\tilde{\mathbf{r}}_{SC/S}(t_k) - \tilde{\mathbf{r}}_{SC/S}(t_{k-1})\right]$ in Eq. (20). The best approach is still under investigation. To avoid processing correlated measurements in the EKF, since the observation time is so short, several measurement cycles are skipped between delta-phase range measurements. The simulation currently processes every 20$^{\text{th}}$ possible measurement.

The accuracy of the absolute and delta-phase range measurement has been shown to depend on pulsar photon flux, pulse period, X-ray background rates, and detector area [33, 34]. Values from these past analyses are provided in Table 1, with some of the delta-phase range values being estimated based upon past and on-going research using Cramer-Rao lower bound photon processing analysis and detailed error budgets with pulse characteristics approaches [33, 34]. These values assume a 1-m^2 detector area. Past analysis has also shown that combining both absolute and delta-phase range measurements can improve the overall XNAV solution. However, for the results presented below, these types of measurements are treated independently.

Table 1. Measurement Accuracies For Simulated XNAV Observations.

Source Name (PSR)	Absolute Range Meas.		Delta-Phase Range Meas.	
	Observ. Length (s)	TOA Range Acc. (km)	Observ. Length (s)	Phase Range Acc. (km)
B1937+21	25,000 100,000	0.16 0.078	100	2*
B1821–24	25,000 100,000	0.20 0.10	100	2*
B0531+21	25,000 100,000	0.027 0.013	100	0.5

* Estimated values

The primary outputs of the simulation are the continuous error between the truth and EKF state solution over the entire simulation run; the estimate of the EKF performance using its computed covariances as a function of time; and a computation of spherical error probable (SEP) along the trajectory. These outputs are used to assess the performance of the EKF during a particular simulation run, and to compare between the different DSN and XNAV EKF implementations.

SIMULATION RESULTS

To provide representative results from this simulation, an interplanetary trajectory between Earth and Mars was selected. By choosing the correct departure date of the mission to produce the proper phasing of the planets in their orbits, along with several TCMs along the trajectory, this type of mission is executed in approximately 300 days. Although the entire trajectory is of interest, it was chosen to investigate the latter portion of the path, during the vehicle's approach to Mars. After the appropriate path injection at the beginning of the mission, and after several TCMs to stay on course, it is of interest to determine how well the navigation solution is maintained as the vehicle approaches its target rendezvous location, in order to establish if any final TCM is required and its magnitude. Smaller TCM burn magnitudes during the interplanetary cruise could mean additional operational life when the vehicle finally arrives at its destination. A plot of the orbits of the inner planets and the space vehicle is shown in Figure 6.

Each simulation is run for 60 days (5,184,000 s) prior to rendezvous at Mars. The integration time step is 1000 s, unless observations are done more frequently, when the time step is reduced to the observation length. Initial values for the standard deviations in each EKF covariance matrix are set to 500 m for position states and 500 mm/s for velocity states.

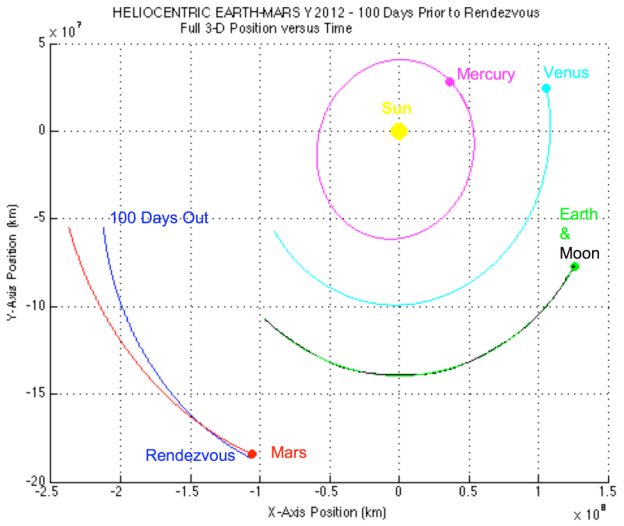

Figure 6. Planetary orbit and spacecraft trajectory plots during last 100 days prior to Mars rendezvous.

DSN ΔDOR observations are processed within the simulation once per day (once every 87000 seconds for simulation simplicity). *A priori* uncertainties in the DSN navigation solution can vary from 1000 km and 1 km/s to 10 m and 10 mm/s depending on the number of preceding observations and how close to the current epoch these were processed. For the analysis presented here, all simulations runs were initiated with 100 m position and 100 mm/s velocity error along each axis, which assumes some amount of solution convergence at this epoch. The objective of each EKF is to maintain this solution, or improve upon it as much as possible based upon its processed observations. The absolute range observations in the XNAV EKF are processed every 25,000 s, along with the uncertainties estimated in Table 1, and delta-phase observations use 100 s observations.

Example performance values of each navigation EKF during an example set of simulation runs are provided below in Table 2 through Table 4. The values of the RMS error of the EKF solution and the mean of the standard deviation (SD) of the EKF covariance matrix are provided for values after a specified duration of filter settling. Values are shown for after 3 days (259,200 s) and 30 days (2,592,000 s) of processing. The axes chosen for these results are the RAC axes that are Earth-centered (not Sun-centered). This is to help show the solution for the DSN observations that are formed relative to Earth. The plots in Figure 7 show the error in the simulated position state and the covariance envelope. The EKF's estimate of position grows rapidly between successive observation updates, where the standard deviation values quickly reduce to small values after each measurement is processed.

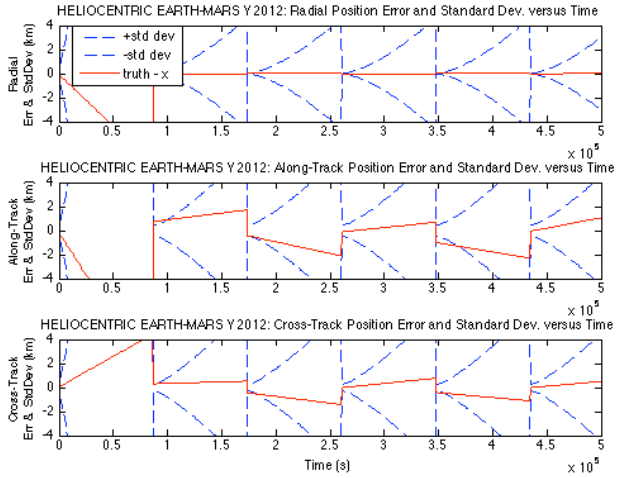

Figure 7. DSN ΔDOR EKF simulation position plots, with state error from truth and covariance envelope.

Although the computed DSN errors in position remain low, less than 1 km, the estimated SD from the EKF is a few km in size in Table 2. As anticipated, the errors are larger along the along-track and cross-track axes, as DSN can produce very accurate radial measurements, but less accurate along the remaining two axes. Some of the terms seem to increase after the 30 days compared to after 3 days, however this is attributed to the specific data from this individual run. The SD terms are the mean over the specified duration, thus this value becomes large in part due to the infrequency of measurements (once per day) and the size of the process noise that drives the increase between measurements.

Table 2. DSN EKF Simulation Performance Values.

State		After 3 Days of Filter Settling		After 30 days of Filter Settling	
		EKF Error RMS	EKF SD Mean	EKF Error RMS	EKF SD Mean
Pos: (m)	R	183	1862	246	1884
	A	941	3039	980	3055
	C	615	2923	671	2939
Vel: (mm/s)	R	0.97	62	1.1	62
	A	12	82	12	82
	C	7.7	81	8.2	81

The results for the absolute and delta-phase range measurements within the XNAV EKF are provided in Table 3 and Table 4. For the relative-phase range processing, the solutions are less accurate than the DSN or absolute-range XNAV processing. This approach can improve the along-track error, since the observation is primarily along this direction for delta-phase changes. However, some of this error is currently due to having two of the three sources with much less accuracy than the Crab, as from Table 1. As source analysis is continuing, other sources are likely more beneficial for this phase tracking approach that produce more source flux than these two, faint pulsars in B1821-24 and B1937+21 used in this analysis. Additional test runs recently completed with 500-m accuracy for each of three sources have shown substantial improvements in the non-radial performance values as listed in Table 3.

Since it is not likely that future missions would be launched without DSN communication and tracking capability, it is interesting to determine the performance of a combined DSN and XNAV solution. To study this, a combined EKF that allows the processing of both DSN and XNAV measurements during the same simulation run has been created. XNAV measurements are made available in between successive DSN measurements produced once per day.

Table 3. XNAV Absolute-Range EKF Simulation Performance Values.

State		After 3 Days of Filter Settling		After 30 days of Filter Settling	
		EKF Error RMS	EKF SD Mean	EKF Error RMS	EKF SD Mean
Pos: (m)	R	1001	6000	965	5917
	A	403	1781	491	2036
	C	808	4076	786	4071
Vel: (mm/s)	R	8.2	97	7.9	97
	A	5.9	64	6.1	65
	C	7.9	83	7.7	83

Table 4. XNAV Delta-Phase Range EKF Simulation Performance Values.

State		After 3 Days of Filter Settling		After 30 days of Filter Settling	
		EKF Error RMS	EKF SD Mean	EKF Error RMS	EKF SD Mean
Pos: (m)	R	1876	4262	1900	4095
	A	681	1417	882	1919
	C	1172	3472	1216	3472
Vel: (mm/s)	R	22	80	22	77
	A	11	47	13	51
	C	15	74	15	74

When adding XNAV absolute-range measurement to DSN ΔDOR processing the noticeable improvement comes from the additional measurements in between DSN measurements, as in Table 5. This considerably reduces the position covariance values so that the along-track and cross-track values are reduced. Additionally, the RMS errors of velocity are reduced along these two axes also. This may identify the primary benefit of XNAV measurements, by providing measurements along axes normal to the radial direction that DSN is primarily very good at observing. Table 6 shows the results of combined DSN and XNAV delta-phase range measurements, showing a marked improvement over the XNAV-only delta-phase range accuracy displayed in Table 4. It is likely that further filter tuning is required to fully optimize the usage of XNAV with DSN processing. However, this initial analysis shows that the powerful benefits of this measurement augmentation. Another method would be to incorporate both absolute-range and delta-phase range measurements along with DSN for a fully integrated system.

Future plans for this analysis include additional deep-space trajectories, including those towards outer planets, such as Earth-Jupiter, or Jupiter-Pluto, and out towards the solar system boundary. Further investigations of X-ray source characteristics and candidates are to be pursued to verify the measurement accuracies and increase the set of available sources. To improve the performance analysis for these systems, a set of simulation runs in a Monte Carlo analysis will be completed. This avoids any specific peculiarities with an individual run, and a preliminary analysis of this type has shown that the existing runs are representative of expected results.

Table 5. Combined DSN and XNAV Absolute-Range EKF Simulation Performance Values.

State		After 3 Days of Filter Settling		After 30 days of Filter Settling	
		EKF Error RMS	EKF SD Mean	EKF Error RMS	EKF SD Mean
Pos: (m)	R	268	1820	312	1849
	A	389	838	422	902
	C	926	2370	990	2413
Vel: (mm/s)	R	4.7	61	5.4	61
	A	13	51	14	51
	C	19	73	20	73

Table 6. Combined DSN and XNAV Delta-Phase Range EKF Simulation Performance Values.

State		After 3 Days of Filter Settling		After 30 days of Filter Settling	
		EKF Error RMS	EKF SD Mean	EKF Error RMS	EKF SD Mean
Pos: (m)	R	1001	1721	1098	1708
	A	314	979	361	1111
	C	1016	2231	1141	2255
Vel: (mm/s)	R	17	59	19	59
	A	8.9	50	9.5	52
	C	18	71	20	72

CONCLUSION

The analysis presented here shows the capabilities of XNAV to support or augment DSN measurements for different types of deep space missions. By combining these methods, performance improvements can be shown compared to either system alone.

The XNAV concept shows remarkable promise to support a wide range of potential NASA missions. For missions to Jupiter and beyond, XNAV promises the potential of improved navigation accuracy relative to current and planned DSN performance, while reducing the demand on the resource-limited DSN tracking network for deep-space probes [33]. For nearer missions (e.g., Mars, Earth-Sun Lagrange L2 point, asteroid belt, large baseline formations), including crewed missions, XNAV could enable long-term autonomy or serve as a robust auxiliary navigation capability. The reduced demands on the DSN combined with the potential for improved navigation accuracy could yield cost savings and mission enhancements to these missions.

Most very deep space missions proposed to date with any level of depth and incorporating existing technology go out to distances of several hundred AU [41, 42]. A mission to investigate the Pioneer gravitational anomaly has been proposed, which would require accurate tracking of the spacecraft to distances far beyond Jupiter, measuring the acceleration of the spacecraft very precisely [43]. XNAV could assist in providing more accurate navigation data than can be obtained from DSN alone, and provide real time solutions onboard the vehicle.

ACKNOWLEDGMENTS

The authors wish to sincerely thank Charles Naudet and Walid Majid of NASA JPL who provided significant contributions to the understanding of the current DSN operation and performance. They also thank the additional members of the NASA technical team for XNAV, including Russell Carpenter and Keith Gendreau of NASA GSFC for their helpful discussions. They would also like to thank Darryll Pines of the University of Maryland for his original contributions to this overall XNAV concept, and Robert Golshan of the Aerospace Corporation, who contributed considerably to the development of the relative-range XNAV measurement concept.

REFERENCES

[1] Jet Propulsion Laboratory, "About The Deep Space Network," [online], California Institute of Technology, NASA, 2008, URL: http://deepspace.jpl.nasa.gov/dsn/ [cited 22 December 2008].

[2] Mudgway, D. J., *Uplink-Downlink, A History of the Deep Space Network 1957–1997*, National Aeronautics and Space Administration, Washington, DC, 2001.

[3] Thornton, C. L., and Border, J. S., *Radiometric Tracking Techniques for Deep Space Navigation*, John Wiley & Sons, Hoboken, NJ, 2003.

[4] Seidelmann, P. K., *Explanatory Supplement to the Astronomical Almanac*, University Science Books, Sausalito CA, 1992.

[5] Standish, E. M., "NASA JPL Planetary and Lunar Ephemerides," [online database], NASA, URL: http://ssd.jpl.nasa.gov/eph_info.html [cited 1 December 2004].

[6] Parkinson, B. W., and Spilker, J. J. J. Eds., *Global Positioning System: Theory and Applications, Volume I*. American Institute of Aeronautics and Astronautics, Washington, DC, 1996.

[7] Moyer, T. D., *Formulation for Observed and Computed Values of Deep Space Network Data Types for Navigation*, John Wiley & Sons, Inc., Hoboken, New Jersey, 2003.

[8] Lanyi, G., Bagri, D. S., and Border, J. S., "Angular Position Determination by Spacecraft by Radio Interferometry," *Proceedings of the IEEE*, Vol. 95, No. 11, IEEE, November 2007.

[9] Naudet, C. J., and Majid, W. A., "DSN Operation and Performance Capabilities," Personal Communication, 2008.

[10] Bhaskaran, S., "The Application of Noncoherent Doppler Data Types for Deep Space Navigation," Jet Propulsion Laboratory, Pasadena, CA, The Telecommunications and Data Acquisition Progress Report 42-121, May 15, 1995.

[11] Downs, G. S., "Interplanetary Navigation Using Pulsating Radio Sources," *NASA Technical Reports N74-34150*, 1974, pp. 1-12.

[12] Chester, T. J., and Butman, S. A., "Navigation Using X-ray Pulsars," *NASA Technical Reports N81-27129*, 1981, pp. 22-25.

[13] Hanson, J. E., "Principles of X-ray Navigation," Doctoral Dissertation, Stanford University, 1996, URL: http://il.proquest.com/products_umi/dissertations/.

[14] Sheikh, S. I., Pines, D. J., Wood, K. S., Ray, P. S., Lovellette, M. N., and Wolff, M. T., "Spacecraft Navigation Using X-ray Pulsars," *Journal of Guidance, Control, and Dynamics*, Vol. 29, No. 1, 2006, pp. 49-63.

[15] Sheikh, S. I., "The Use of Variable Celestial X-ray Sources for Spacecraft Navigation," Ph.D. Dissertation, University of Maryland, 2005, URL: https://drum.umd.edu/dspace/handle/1903/2856.

[16] Sheikh, S. I., and Pines, D. J., "Recursive Estimation of Spacecraft Position and Velocity Using X-ray Pulsar Time of Arrival Measurements," *Navigation: Journal of the Institute of Navigation*, Vol. 53, No. 3, 2006, pp. 149-166.

[17] Sheikh, S. I., Pines, D. J., Wood, K. S., Ray, P. S., Lovellette, M. N., and Wolff, M. T., "The Use of X-ray Pulsars for Spacecraft Navigation," *14th AAS/AIAA Space Flight Mechanics Conference*, Paper AAS 04-109, Maui HI, February 8-12 2004.

[18] Baade, W., and Zwicky, F., "On Super-novae," *Proceedings of the National Academy of Science*, Vol. 20, No. 5, 1934, pp. 254-259.

[19] Baade, W., and Zwicky, F., "Cosmic Rays from Super-novae," *Proceedings of the National Academy of Science*, Vol. 20, No. 5, 1934, pp. 259-263.

[20] Oppenheimer, J. R., and Volkoff, G. M., "On Massive Neutron Cores," *Physical Review*, Vol. 55, 1939, pp. 374-381.

[21] Hewish, A., Bell, S. J., Pilkington, J. D., Scott, P. F., and Collins, R. A., "Observation of a Rapidly Pulsating Radio Source," *Nature*, Vol. 217, 1968, pp. 709-713.

[22] Charles, P. A., and Seward, F. D., *Exploring the X-ray Universe*, Cambridge University Press, Cambridge UK, 1995.

[23] White, N. E., Nagase, F., and Parmar, A. N., "The Properties of X-ray Binaries," *X-ray Binaries*, W. H. G. Lewin, J. van Paradijs, and E. P. J. van den Heuvel Eds., Cambridge University Press, Cambridge UK, 1995, pp. 1-57.

[24] Kaspi, V. M., Taylor, J. H., and Ryba, M. F., "High-Precision Timing of Millisecond Pulsars. III: Long-Term Monitoring of PSRs B1855+09 and B1937+21," *Astrophysical Journal*, Vol. 428, 1994, pp. 713-728.

[25] Matsakis, D. N., Taylor, J. H., and Eubanks, T. M., "A Statistic for Describing Pulsar and Clock Stabilities," *Astronomy and Astrophysics*, Vol. 326, 1997, pp. 924-928.

[26] Sala, J., Urruela, A., Villares, X., Estalella, R., and Paredes, J. M., "Feasibility Study for a Spacecraft Navigation System relying on Pulsar Timing Information," European Space Agency Advanced Concepts Team ARIADNA Study 03/4202, 23 June 2004.

[27] Sheikh, S. I., Golshan, A. R., and Pines, D. J., "Absolute and Relative Position Determination Using Variable Celestial X-ray Sources," *30th Annual AAS Guidance and Control Conference*, pp. 855-874, American Astronautical Society, Breckenridge, CO, 3-7 February 2007.

[28] Manchester, R. N., and Taylor, J. H., *Pulsars*, W.H. Freeman and Company, San Francisco CA, 1977.

[29] Lyne, A. G., and Graham-Smith, F., *Pulsar Astronomy*, Cambridge University Press, Cambridge UK, 1998.

[30] Fraser, G. W., *X-ray Detectors in Astronomy*, Cambridge University Press, Cambridge UK, 1989.

[31] Taylor, J. H., "Pulsar Timing and Relativistic Gravity," *Philosophical Transactions of the Royal Society of London*, Vol. 341, 1992, pp. 117-134.

[32] Wood, K. S., "Navigation Studies Utilizing The NRL-801 Experiment and the ARGOS Satellite," *Small Satellite Technology and Applications III*, Ed. B. J. Horais, International Society of Optical Engineering (SPIE) Proceedings, Vol. 1940, 1993, pp. 105-116.

[33] Hanson, J., Sheikh, S., Graven, P., and Collins, J., "Noise Analysis for X-ray Navigation Systems," *IEEE-ION Position Location and Navigation Symposium (PLANS) 2008*, Monterey, CA, 5-8 May 2008.

[34] Golshan, A. R., and Sheikh, S. I., "On Pulse Phase Estimation and Tracking of Variable Celestial X-Ray Sources," *Institute of Navigation 63rd Annual Meeting*, Cambridge, MA, April 23-25, 2007.

[35] Ashby, N., and Golshan, A. R., "Minimum Uncertainties in Position and Velocity Determination Using X-ray Photons From Millisecond Pulsars," *Institute of Navigation National Technical Meeting*, San Diego, CA, 28-30 January 2008.

[36] Graven, P., Collins, J., Sheikh, S., and Hanson, J. E., "XNAV Beyond the Moon," *Institute of Navigation 63rd Annual Meeting*, Cambridge, MA, April 23-25, 2007.

[37] Graven, P. H., Collins, J. T., Sheikh, S. I., and Hanson, J. E., "Spacecraft Navigation Using X-ray Pulsars," *7th International ESA Conference on Guidance, Navigation, & Control Systems*, GNC 2008, Tralee, County Kerry, Ireland, 2-5 June 2008.

[38] Shanks, E. B., "Solutions of Differential Equations by Evaluations of Functions," *Mathematics of Computation*, Vol. 20, No. 93, 1966, pp. 21-38.

[39] Brown, R. G., and Hwang, P. Y. C., *Introduction to Random Signals and Applied Kalman Filtering*, Third ed., John Wiley and Sons, New York, 1997.

[40] Vallado, D. A., *Fundamentals of Astrodynamics and Applications*, Second ed., Space Technology Library, Kluwer Academic Publishers, Boston MA, 2001.

[41] Mewaldt, R. A., and Liewer, P. C., "An Interstellar Probe Mission to the Boundaries of the Heliosphere and Nearby Interstellar Space," [online], URL: http://interstellar.jpl.nasa.gov/interstellar/ISP_Space2K_v4.pdf [cited 22 December 2008].

[42] Turyshev, S. G., and Andersson, B.-G., "The 550 AU Mission: A Critical Discussion," *Monthly Notices of the Royal Astronomical Society*, Vol. 341, No. 2, 2003, pp. 577-582.

[43] Nieto, M. M., "The Quest to Understand the Pioneer Anomaly," in *europhysicsnews*, Vol. 37, 2006, pp. 30-34.